Self-Applied Magnetic Field Effects on Solid Propellant MPD Thruster Performance*

Giorgio Paccani and Luigi Petrucci
Università degli Studi di Roma "La Sapienza"
Dipartimento Meccanica e Aeronautica,
Via Eudossiana 18, 00184 Rome, Italy.
Rome Italy
+39.06.44585283
g.paccani@dma.ing.uniroma1.it

IEPC-01-140

The effects of different self-applied axial magnetic fields on the behavior of a coaxial solid propellant MPD thruster have been examined. The self-applied magnetic fields were generated by coaxial external coils, respectively a shorter six-turn coil mounted in three different axial positions and a longer six-turn coil having the same length as the acceleration duct. Measurements, performed at six different power levels, included electrical characteristics, impulse bit (thrust stand), exhaust velocity (TOF Langmuir probe system), and ablated propellant mass per shot. A comparison at equal current parameter shows that higher currents, i.e. higher self-applied magnetic fields, lead to higher ablated mass, smaller jet exhaust velocities, and higher impulse bit. The self-applied magnetic field due to the short coil in the most upward position was the least effective, whilst the other configurations exhibited comparable performance.

Nomenclature

MPD	Magnetoplasmadynamic
PFN	Pulse forming network
PVC	Polyvinyl chloride
TOF	Time of flight

Symbols

B	Magnetic field, T
C	Capacitance, C
E	Energy, J
I_b	Impulse bit, N s
i	Current, A
J	Current density, A/m^3
K	Ψ/m, A^2 s/Kg
m	Ablated mass per shot, Kg
P	Power, W
r	Radius, mm
t	Time, s
T	Thrust, N
V	Potential, V
w	Exhaust velocity, m/s
Z	Impedance, Ω
η	Efficiency
τ	Discharge duration, s
Ψ	Current parameter, $\int i^2 \, dt$, A^2 s

Subscripts

r	Radial component
t	Thrust
th	Theoretical
z	Axial component
θ	Azimuthal component
0	Initial or set value

Introduction

This paper deals with coaxial solid propellant ablative MPD thrusters operating in pulsed mode with instantaneous power levels of a few megawatts during pulses (shots) which last approximately one millisecond.

This class of electromagnetic thruster provide relatively high specific impulse in a simple, robust design along with a well-defined impulse bit delivery capability. Its performance is determined by engine scale[1], thruster geometry[2,3], arc and propellant properties[4,5,6] and arc-propellant interaction[7,8], being the propellant flow rate determined by the propellant mass rate ablated from the discharge.

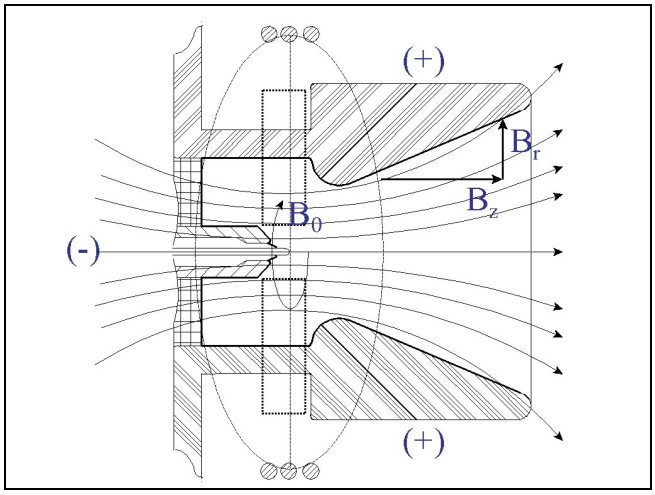

Figure 1 - Self-induced (B_θ) and self-applied (B_z) magnetic fields.

Applying an external axial magnetic field (Fig. 1) is known to affect MPD thrusters behavior[9-17] improving their performance. In the coaxial thrusters, such an external field can be generated by a coaxial coil surrounding a part of the discharge chamber and inserted in the current path of the propulsive system. The same current forming the discharge flows, through the coil generating a "self-applied" external magnetic field. The interaction between this external magnetic field and the discharge causes a plasma swirling motion around the thruster axis.

Previous studies[17] were carried out on the impact of a self-applied magnetic field on the behavior of ablative MPD thrusters (electrical characteristics and performance), while varying the discharge chamber geometry, the anodic configuration and the axial position of the magnetic field. The effects of the self-applied magnetic field due to a two-turn coil became more important augmenting the input energy, i.e. augmenting the magnitude of the magnetic field itself. Also the axial position of the coil influenced the behavior of the thruster.

Therefore, this paper will describe and discuss the results of an experimental activity aimed at investigating the effects of an increased magnetic field due to six-turn coils. Two coils were used:

- a shorter coil, whose axial length is about one third the length of the acceleration duct; it was mounted in three axially different positions (Fig. 2);
- a longer coil, whose axial length extends for 7/9 of the acceleration duct starting from the cathode tip (Fig. 2).

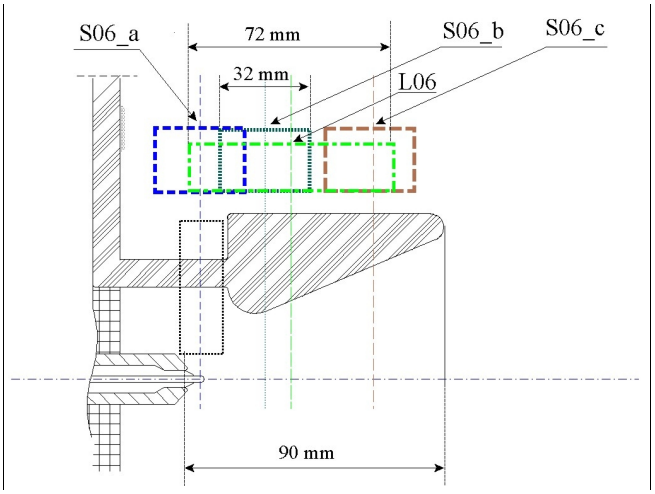

Figure 2 - Dimensions and positions of the coils: the long one, L06, and the short one in the three configurations S06_a, S06_b, S06_c.

Electrical characteristics, impulse bit (thrust stand), exhaust velocity (TOF Langmuir probe system), and ablated propellant mass per shot were measured.

Experimental Setup

The propulsive systems and the facilities used for the experiments are summarized in this section. The test procedures and measurements are also covered.

Propulsive System

The MPD propulsive system consists of energy storage means, a coaxial transmission line, an accelerator (with or without coil) and a start-up circuit.

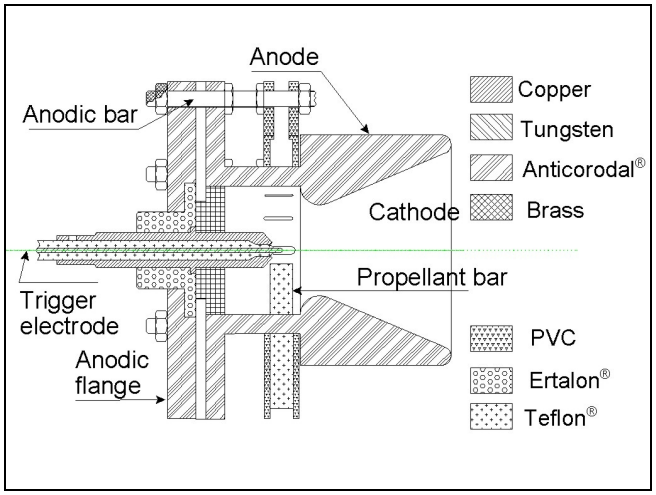

Figure 3 - Baseline MIRA solid propellant thruster.

The baseline thruster configuration (Fig. 3), denoted MIRA, is described in detail elsewhere[18,19]. Briefly, the MIRA thruster has a "discharge chamber" delimited by an anode-nozzle with an exit radius of about 55 mm and an area ratio of 5.5 to 1 which co-axially surrounds a cylindrical-conical cathode with a diameter of 18 mm. The anode-nozzle is fabricated using an aluminum-silicon-manganese-alloy while the cathode is made of copper. Six Teflon® propellant bars pass radially through the wall of the anode and symmetrically surround the cathode tip. A 2 mm-diameter trigger electrode, which is located co-axially within the thruster cathode is used to initiate the discharge. The trigger electrode is insulated from the thruster cathode by a sleeve of Teflon®. The discharge is initiated by a 0 to 20 KV power supply connected to the tungsten trigger electrode and the cathode.

The coils, described in detail elsewhere[18, 19], consist (Figs. 4, 5) respectively of six copper cables, with a section of 2.5 mm^2, wrapped around a cylinder of PVC. At its ends, two 2.5 mm thick copper flanges are mounted. Six brass conductors connect the coil to the anodic feeding of the thruster ("in-going" conductors) while six others connect it to the discharge chamber-anode-nozzle ("out-going" conductors).

The wrapping of each of the cables can be considered equivalent to a six-turn coil; it has a length of about 32 mm with a mean radius of about 75 mm in the short coil and a length of about 72 mm with a mean radius of about 69 mm in the long coil.

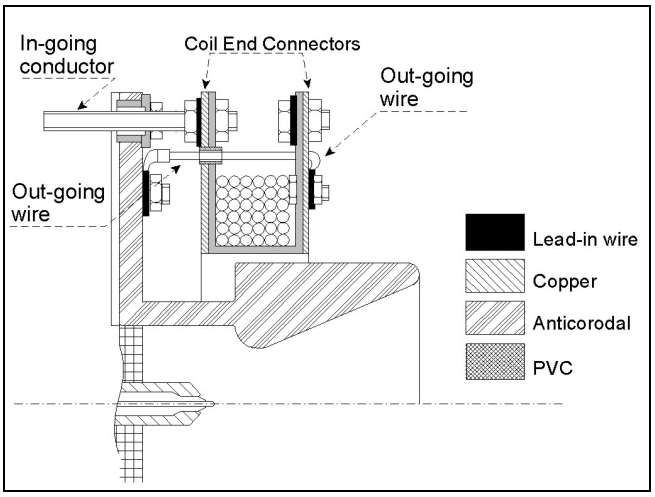

Figure 4 - Sketch of a partial view of the short coil mounted on the thruster.

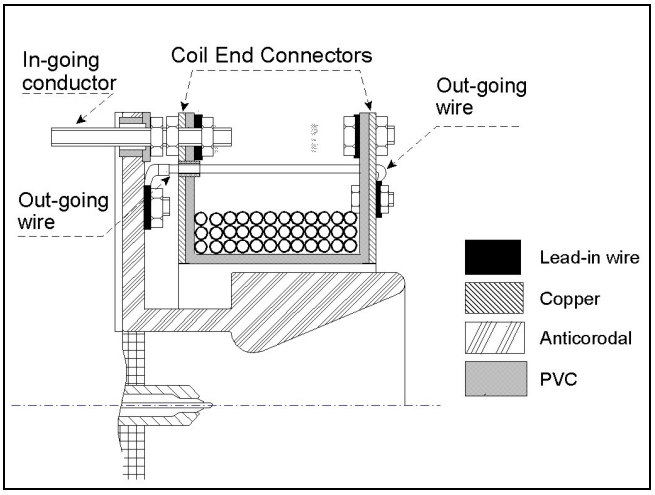

Figure 5 - Sketch of a partial view of the long coil mounted on the thruster.

The thruster constituted by the MIRA thruster assembled with the short coil is denoted in general MIRA_S06_x: in particular respectively MIRA_S06_a, MIRA_S06_b, MIRA_S06_c depending on the axial position of the coil (Fig. 2). The thruster constituted by the MIRA thruster assembled with the long coil is denoted MIRA_L06.

The energy storage means consist of a capacitive pulse forming network (PFN) with a total capacitance of 0.072 ± 0.002 F split into two 15-capacitor branches; it is connected to the thruster electrodes by a coaxial line. The PFN set voltage was the primary externally controllable variable during the tests.

Test Facilities

The tests were conducted in a 0.5 m^3, polyvinyl chloride (PVC) vacuum tank with a nominal back pressure of 10^{-2} Pa. All the instrumentation was housed in a full Faraday cage and data acquisition was computer-controlled.

Measurements and Test Procedures

Experimental direct measurements included the instantaneous electrical characteristics [PFN potential difference, $V(t)$, and discharge current intensity, $i(t)$], impulse bit, I_b, ion velocity in the exhaust jet, w, and ablated propellant mass, m.

The potential was measured directly using an oscilloscope while current was measured using a Rogowsky probe. A value averaged over 12 measurements was used as the standard value for each electrical parameter. The energy per shot

$$E_T = \int_0^\infty i(t) \cdot V(t)\, dt . \qquad (1)$$

was computed using the measured electrical parameters.

A thrust balance, described in detail elsewhere[20], was used to measure the thruster impulse bit.

The ablated propellant mass was obtained by weighing the propellant bars before and after series of shots using an electronic balance. Taking into account the amount of the measured mass differences (> 75 mg), the balance accuracy (± 1 mg), the material deposition on the propellant bars and the propellant handling, the error in this measurement has been estimated to be a maximum of ±5 mg.

Finally, the jet exhaust velocity was measured based upon the average value of 30 time of flight (TOF) measurements. Velocities were obtained[21] from cross correlation of the signals from two double Langmuir probes located on the axis of the jet downstream of the thruster.

Errors/uncertainties were calculated using error propagation theory based on the standard deviation of the individual measurements.

Each of the thrusters has been tested at six different regimes. The regimes were characterized by the initial energy stored in the PFN, E_0; this was fixed in increments of 333 J from 1333 J to 3333 J by setting the PFN potential, V_0, according to

$$E_0 = \frac{1}{2} C V_0^2 . \qquad (2)$$

Experimental Results

To thoroughly analyze the behavior of the thrusters, the characteristic parameters will be analyzed while varying energy, E_T, and current parameter, Ψ.

The energy, E_T, is the fraction of the stored energy, E_0, actually employed in the thruster+transmission line system. Ψ represent an index of the squared current intensity in the discharge chamber regardless of electrical losses in the circuit. Then the parameter characteristics as a function of the energy, E_T, provide information on the functioning of the system thruster+transmission line

while graphs reported as a function of the current parameter, Ψ, provide information on the behavior of the only discharge event inside the discharge chamber. Therefore, in order to examine in particular the acceleration process, we will present in the subsequent discussions, the results as a function of Ψ unless the use of E_T enables additional insights.

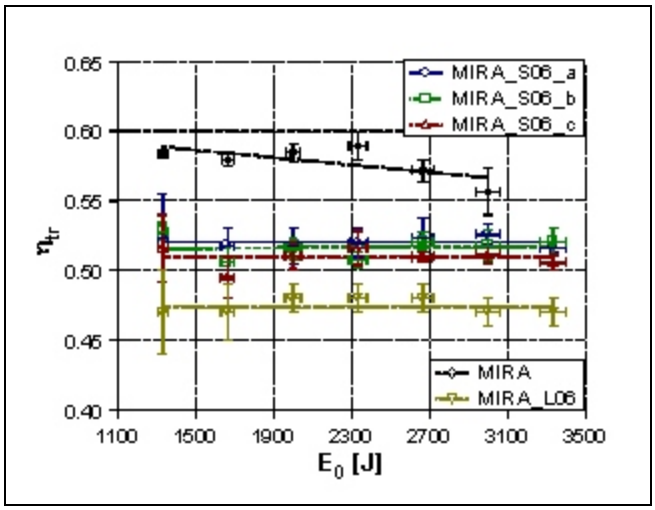

Figure 6 - Transmission efficiency, η_{tr}, as a function of input energy, E_0, shows constant behaviors.

The different propulsive systems (PFN + transmission line + thruster) result from the coupling of the same PFN and transmission line with different thrusters having different impedance. The insertion of the coil augments the impedance of the truster. On the other hand the magnetic field created by the coil can change the plasma conductivity. As a consequence the propulsive systems have electrical behavior which are considerably different from one another depending on the coil.

The systems with coil exhibit a transmission efficiency

$$\eta_{tr} = \frac{E_T}{E_0}$$

constant regardless of the input energy, E_0, while the baseline thruster MIRA shows an efficiency which slightly decreases with increasing input energy (Fig. 6).

The values of the MIRA_S06_x thrusters (thrusters with short coils), very close to one another, are higher than the MIRA_L06 ones and lower than the MIRA ones.

Current parameter

Energy, E_T, and current parameter show linear increases as a function of input energy, E_0. When cross-plotting the energy, E_T, and current parameter, Ψ, the behavior is strictly linear (Fig. 7).

As expected, due to the coil impedance, the baseline thruster MIRA shows values of the current parameter, at constant E_T, much higher than the self-applied magnetic field configurations. The latter exhibit values very close to one another. Nevertheless the following inequality is obeyed:

$$\Psi_{MIRA} >> \Psi_{MIRA\_S06\_c} \geq \Psi_{MIRA\_S06\_a} \geq \Psi_{MIRA\_S06\_b} = \Psi_{MIRA\_L06}.$$

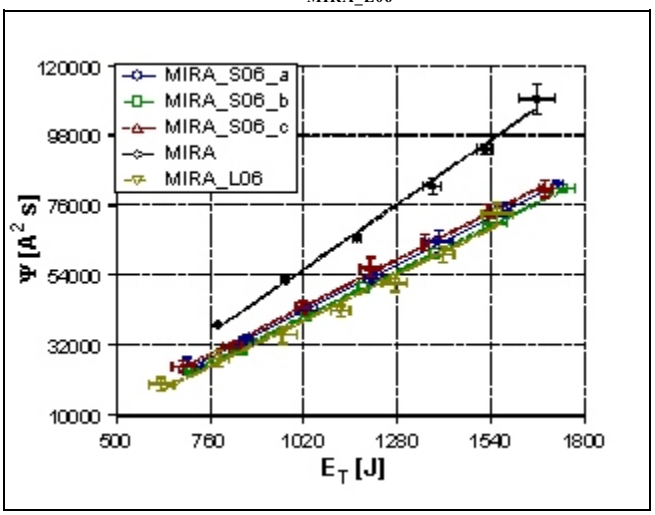

Figure 7 - Current parameter, Ψ, as a function of energy, E_T, shows a linear relationship.

Impedance

The impedance of thruster and transmission line exhibits similar behavior when augmenting E_T and Ψ. In both cases it shows a parabolic decrease while tending towards a limiting constant value (Fig. 8). For constant E_T and Ψ, in consistency with the current parameter characteristics, the impedance characteristics obey the

following inequality:

$$Z_{MIRA\_L06} \geq Z_{MIRA\_S06\_b} \geq Z_{MIRA\_S06\_a} \geq Z_{MIRA\_S06\_c} >> Z_{MIRA}.$$

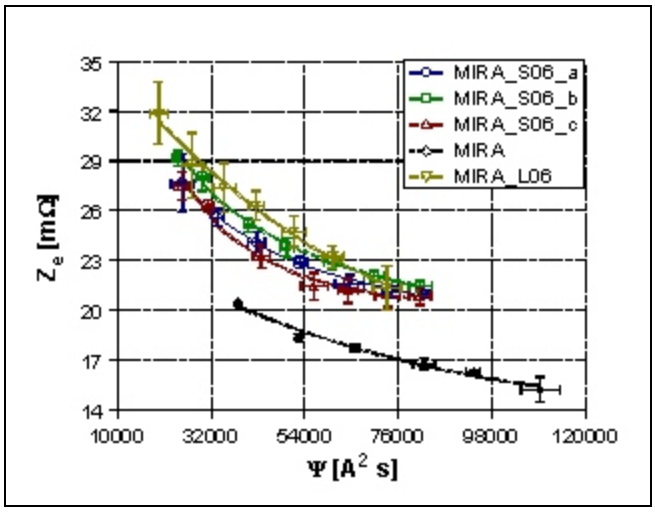

Figure 8 - Thruster and transmission line impedance, Z_e, versus current parameter, Ψ, shows the tendency towards a lower limiting constant value with increasing energy.

Ablated mass

In the baseline MIRA, the ablated propellant mass per shot increases linearly with increasing energy, E_T, and current parameter, Ψ (Fig. 9). This does not hold true for the configurations with coil. In particular the MIRA_S06_c shows two clearly different behaviors: for low values of the current parameter (Ψ ≈ 2000-7000 A^2s) it exhibits the lowest consumption of all analyzed thrusters, while at higher values of the current parameter (Ψ ≈ 7000-9000 A^2s) it presents the highest ablated mass. Generally speaking, the thrusters with the short coil show steeper slopes than the baseline thruster; the slope increases moving the coil downstream along the axis of the thruster. The configurations MIRA_L06 and MIRA_S06_b show again almost the same values.

At constant Ψ, both in terms of absolute values and slopes, the ablated mass characteristics obey the following inequality:

$$m_{MIRA\_S06\_x} = m_{MIRA\_L06} > m_{MIRA}.$$

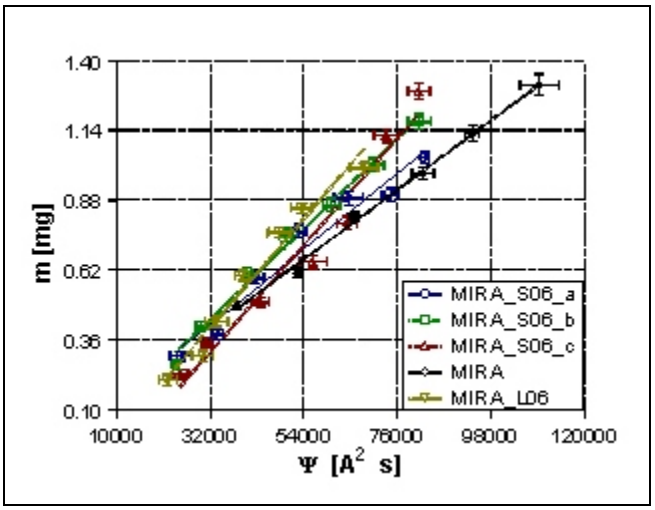

Figure 9 - The linear behavior of the ablated mass per shot, m, as a function of current parameter, Ψ.

K parameter

The parameter

$$K = \frac{i^2}{\dot{m}} = \frac{\Psi}{m}. \qquad (3)$$

represents a qualitative index of the ionization degree of the plasma: the higher the K parameter, the higher the ionization degree up to the on-set condition. In the range of energies within which the thruster exhibits its best behavior, the K parameter of the ablative thrusters is generally almost constant though exhibiting small irregularities[2, 3] (Fig. 10).

The thrusters with coil exhibit a slightly decreasing trend tending to a constant value at higher energies. Among the different thrusters, consistent with the propellant consumption behaviors, the MIRA_S06_c shows the highest values at the lower energies, and the lowest values at the higher energies.

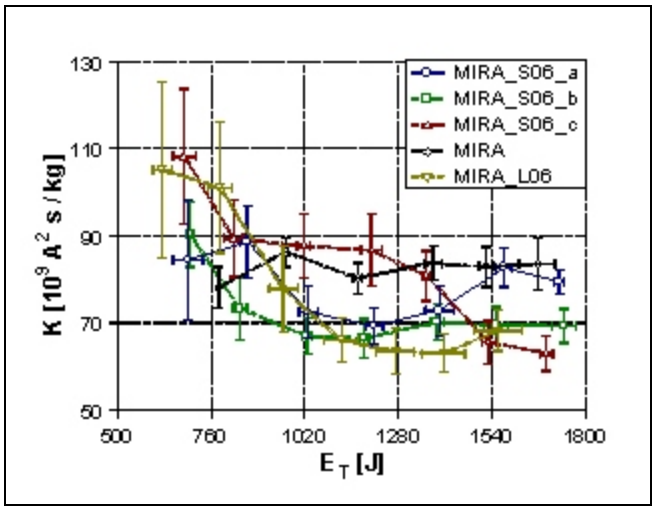

Figure 10 - The self-applied magnetic field changes the behavior of the K parameter as a function of energy, E_T.

Jet Exhaust Velocity

The axial ion exhaust velocity, as already noted in this type of thruster[1,4], shows a general trend towards decreasing velocity as both E_T and Ψ increase (Fig. 11).

The baseline MIRA exhibits a slightly decreasing behavior, while the four configurations with coil show a parabolic decrease while tending towards the same limiting constant value.

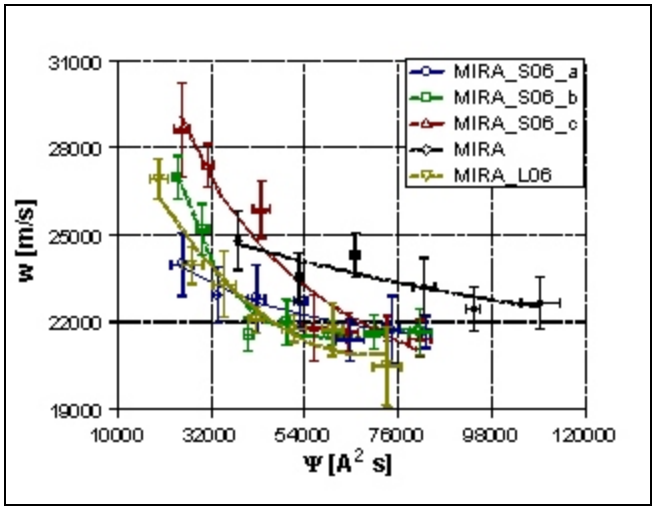

Figure 11 - Ion exhaust velocity shows substantial data scatter and a tendency to decrease with increasing Ψ.

Impulse Bit

Impulse bit increases linearly as a function of both energy, E_T, (Fig. 12) and current parameter, Ψ (Fig. 13). A comparison at constant energy shows:

$$(I_b)_{MIRA} > (I_b)_{MIRA\_S06\_c} \geq (I_b)_{MIRA\_L06} = (I_b)_{MIRA\_S06\_b} > (I_b)_{MIRA\_S06\_a}$$

while a comparison at constant current parameter shows:

$$(I_b)_{MIRA\_L06} = (I_b)_{MIRA\_S06\_b} \geq \geq (I_b)_{MIRA\_S06\_c} > (I_b)_{MIRA} \geq (I_b)_{MIRA\_S06\_a} .$$

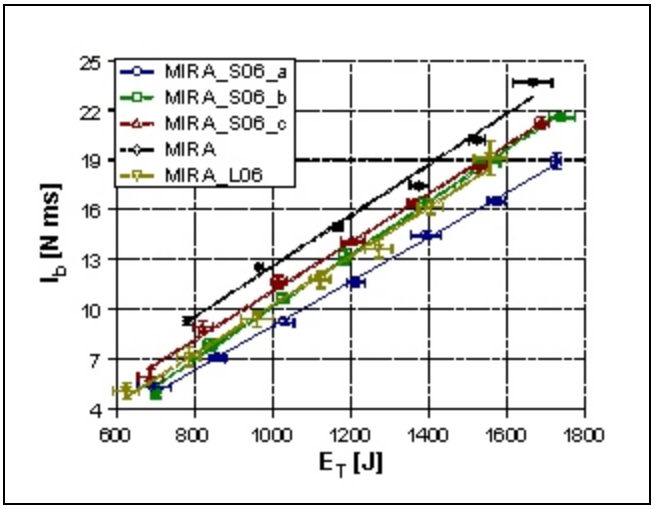

Figure 12 - Linear behavior of impulse bit, I_b, as a function of energy, E_T .

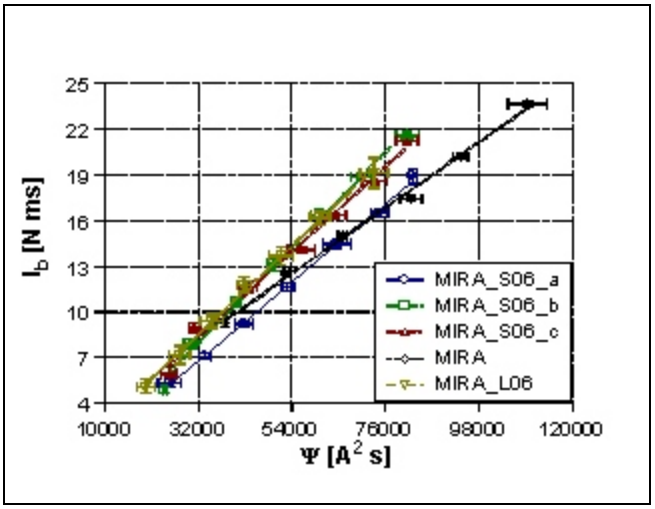

Figure 13 - Linear behavior of impulse bit, I_b, as a function of current parameter, Ψ .

Thrust Efficiency

The thrust efficiency,

$$\eta_T = \frac{I_b^2}{2\,m\,E_T}, \qquad (4)$$

appears to be widely scattered, as seen in previous studies[1,6] (Fig. 14). Like the parameter K, the baseline MIRA shows an almost constant characteristic, while the MIRA_S06_c again exhibits two different behaviors depending on the value of the energy, E_T. The other two configurations with the short coil show increasing values with increasing energy, E_T.

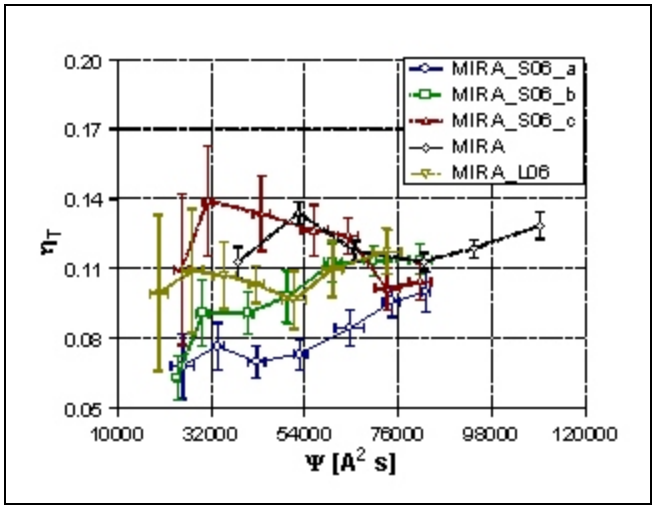

Figure 14 - Thrust efficiency significant data scatter as a function of current parameter.

General Remarks

The minimum thrusters working power level used in the experiments constitutes the threshold level under which the MIRA thruster shows irregular functioning. Moreover, apart from the power level, this thruster showed, in a total random way, some rare "anomalous" shots, i.e. shots in which the values of the parameters were largely different from their average value.

The thrusters with the self-applied magnetic field showed a smoother functioning than the baseline thrusters - no "anomalous" shots - even if their operating power range extends under the inferior threshold level of the MIRA thruster.

In the thrusters with coil the propellant bars show traces of an asymmetric ablation-deposition process, after a series of shots (Fig. 15). Traces of carbonous material deposition were wider on the face of the bars facing the expected direction of the swirling motion of the plasma.

Through the traces left on the anode of the thruster by the discharge, it has been observed that the self-applied magnetic field tends to move the section of the anode stroke by the discharge downstream.

In particular, in the MIRA_S06_a the section of the anode struck by the discharge is around half of the divergent; in the MIRA_S06_b it moves to the end of the anode while in the MIRA_S06_c and in the MIRA_L06 the discharge was found to strike the outside of the thruster. To avoid such occurrence, the external surface of the anode has been insulated. In this way, the discharge was forced to strike the terminal region of the internal surface.

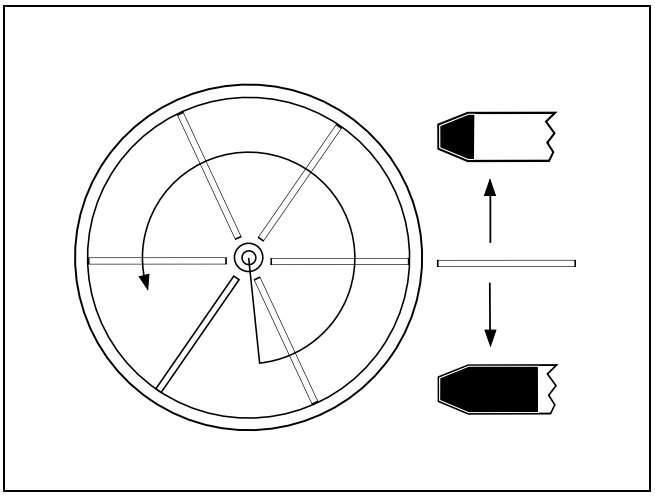

Figure 15 - Carbonous residues on the propellant bars.

Discussion

The asymmetric ablation-deposition process of the propellant bars confirms the presence of both an azimuthal current and a swirling motion of the plasma due to the interactions between the self-applied magnetic field and the component of the discharge current density orthogonal to it.

The anomalous shots in the MIRA thruster are thought to be due to discharge asymmetry; this is caused mostly by longitudinal asperities on the surface of the anode-nozzle generated by localized processes of carbonous residues erosion/deposition. The latter is due to the plasma moving along the anode surface with a high axial velocity.

The plasma swirling motion provides an azimuthally more uniform distribution of the asperities and therefore a more uniform discharge.

The shifting downstream of the discharge along the anode is due to the fact that the plasma electrons tend to follow the self-applied magnetic field: the magnetic field lines are converging upstream of the coil and diverging downstream of the coil (Fig. 1). Therefore, these electrons reach the anode after the middle section of the coil. In the case of the MIRA_S06_c, the magnetic lines do not diverge enough to intersect the internal anode surface, so the electrons reach the external surface.

Electrical Parameters

The electrical parameters are dominated by the influence of the coil: the configurations with coil show very similar values that are quite different from the ones of the baseline thruster. The little difference between the long and the short six-turn coil shows that, once the discharge has been forced to strike the inside of the anode-nozzle, the magnetic field generated in the two cases has practically the same influence on the discharge.

Ablated Mass

It is well-known that the ablation process of a solid material surface occurs when the energy of the plasma surrounding the surface exceeds a threshold value, depending on the material. Moreover the intensity of this process increases with the velocity of the plasma along the surface of the ablated material.

Let's consider now the thrusters with coil. In these thrusters:

- at the lowest power level, only a limited region of the propellant surface is biased by plasma which energy exceeds the threshold value.
- the ablation process is enhanced by the swirling motion of the plasma and the azimuthal current.

Both the swirling motion and the azimuthal current increase with the applied magnetic field, i.e. with Ψ (or thruster working power) and with the angle between the discharge current density and the applied magnetic field direction. In the region surrounding the propellant, when the coil is moved downstream, this angle increases and the applied field decreases. At lower currents the applied field is weak; with increasing currents, it reaches a threshold value over which the swirling motion becomes efficient in the ablation process.

All these considerations can justify the higher values of the ablated mass at equal Ψ and the steeper slopes when Ψ is increased, which were observed in the thrusters with coil (see Fig. 9) as well as the increasing slopes when the coil is moved downstream.

The similarity of the values exhibited by the MIRA_S06_b and those of the MIRA_L06 at the same current, indicates that the interaction between the discharge and the magnetic field (self-applied and self-induced) are similar in the two thrusters, at least in the region where the discharge interacts with the propellant.

Jet Exhaust Velocity

The characteristics of the exhaust velocity are generally consistent with the K parameter but, in the thrusters with coil, the decrease of the velocity with increasing energy is bigger than expected. This is due primarily to a decrease of the ionization of the plasma, consequent to the observed higher ablation of propellant at the same current.

Impulse Bit

At constant current, the azimuthal current interacting with the self-applied magnetic field indirectly augments the thrust generated by the MPD thrusters[22].

Consistently with the above, at constant Ψ, the impulse bit, of the MIRA_S06_b, MIRA_L06 and MIRA_S06_c are all higher than the impulse bit of the baseline thruster and of the MIRA_S06_a (minimum value of azimuthal current).

As already noted, MIRA_S06_b and MIRA_L06 have almost the same values, in consistency with the results of the previous paragraphs.

The higher impedances, i.e. the higher energy losses, accounts for the higher measured values of the impulse bit of the baseline thruster MIRA with respect to the values of the thrusters with coil, at constant energy, E_T.

Summary and Conclusions

Solid propellant with self-applied magnetic field MPD thruster behavior was examined. Five thrusters were tested: a baseline thruster with coaxial electrodes and six radially-mounted propellant bars surrounding the cathode; three thrusters built by assembling the baseline thruster with an axially short coil and one thruster built by assembling the baseline thruster with an axially long coil. Since the coils form a part of the current path , the same current flowing in the discharge flows through the coils.

Measurements included electrical characteristics, impulse bit (thrust stand), exhaust velocity (TOF Langmuir probe system), and ablated propellant mass per shot.

The focus of the test program was to evaluate the effect of the self-applied magnetic field on the thruster performance as functions of E_T energy and Ψ parameter, while varying the coils and their axial position.

The addition of the coils leads, in all cases, to higher impedances and different jet exhaust velocities with a much more regular functioning.

The applied magnetic field causes, at equal Ψ, higher ablated mass and, adopting suitable geometries and positions of the coil, higher impulse bit.

At equal E_T energy, the addition of the coils causes lower impulse bit due to the coil impedance; the use of superconducting wires may remedy this problem.

Acknowledgements

We would like to thank C. Chingari for the precision with which he fabricated the all of the thruster components.

The funding provided by the Italian Space Agency (ASI) and the Italian Ministry of Research (MURST) is gratefully acknowledged.

References

[1] Paccani G., Petrucci L. and Deininger W. D., “Scale Effects On Solid Propellant MPD Thruster Performance”, *AIAA Paper 98-3473, 34th JPC, Cleveland, Ohio (USA),* July 1998.

[2] Paccani G.: "Anode-Nozzle Experimental Analysis in a Coaxial non Steady Solid Propellant MPD Thruster", *IEPC Paper 88-076, 20th IEPC, Garmisch-Partenkirchen, Germany,* October 1988.

[3] Paccani G., Petrucci L. and Deininger W. D., "Experimental Analysis of a Solid Propellant MPD Thruster with Different Anode Radii", *IEPC Paper 99-235, 26th IEPC., Kitakyushu, Japan,* October 1999.

[4] Paccani G., "A Coaxial Non-Steady Solid Propellant MPD Thruster Experimental Analysis", *IEPC Paper 87-1095. 19th IEPC, Colorado Springs, Colorado (USA),* May 1987. - *Journal of the British Interplanetary Society Vol. 41, pp. 253-240,* 1988.

[5] Paccani G., "Experimental Analysis of a Coaxial Solid Propellant MPD Thruster with Segmented Anodes", *IEPC Paper 93-159, 23rd IEPC, Seattle, Washinghton (USA),* September 1993.

[6] Paccani G., Chiarotti U. and Deininger W. D., "Quasi-Steady Ablative Magneto-plasmadynamic Thruster Performance with Different Propellants", *Journal of Propulsion and Power, Vol..14, No. 2, pp. 254-260.* March-April 1998.

[7] Paccani G., "Non-Steady Solid Propellant MPD Thruster Experimental Analysis Concepts", *IEPC Paper 90-2674, 21st IEPC, Orlando, Florida (USA)*, July 1990.

[8] Paccani G., "Studi sui Meccanismi Fisici di Base nei Propulsori MPD"; *ASI 92-RS-27 Report n 1,* April 1993 (In Italian).

[9] Krülle G. and Zeyfang E., "Preliminary Conclusions of Continuous Applied Field Electromagnetic Thruster Research at DFVLR", *AIAA paper 75-417, 11th IEPC, New Orleans, Louisiana (USA),* March 19-21, 1975.

[10] Sasoh A., Solem A. E., and Arakawa Y., "Optimization of Current Distribution in an Applied-Field MPD Thruster". *IEPC Paper 88-057, 20th IEPC, Garmisch-Partenkirchen, W. Germany,* October 3-6, 1988.

[11] Tahara H., Sasaki M., Kagaya Y. and Yoshikawa T., "Thruster Performance and Acceleration Mechanisms of a Quasi-steady Applied Field MPD Arcjet", *AIAA Paper 90-2554, 21st IEPC, Orlando, Florida (USA),* July 18-20, 1990.

[12] Myers R. M., Mantenieks M. and Sovey J., "Geometric Effects in Applied-Field MPD Thrusters". *AIAA Paper 90-2669, 21st IEPC, Orlando, Florida (USA),* July 18-20, 1990.

[13] Sasoh A., "Thrust Formula for an Applied-Field MPD Thruster Derived from Energy Conservation Equation". *IEPC Paper 91-062, 22nd IEPC, Viareggio, Italy,* October 14-17, 1991.

[14] Lawless J. L. and Subramaniam V. V., "A Review of the Theory of Self-Field MPD Thrusters", *IEPC Paper 91-019, 22nd IEPC, Viareggio, Italy,* October 14-17, 1991.

[15] Sasoh A. and Arakawa Y.: "Electromagnetic Effects in an Applied-Field Magnetoplasmadynamic Thruster", *Journal of Propulsion and Power, Vol. 8, No. 1,* January 1992.

[16] York T. M., Zakrzwski C. and Soulas G., "Diagnostics and Performance of a Low-Power MPD Thruster with Applied Magnetic Nozzles", *Journal of Propulsion and Power, Vol. 9, No. 4,* July-August, 1993.

[17] Paccani G.: "Solid-propellant Quasi-steady Mpd Thrusters with Self-Applied Magnetic Field", *32nd JPC, Lake Buena Vista, FL (USA),* July 1-3, 1996.

[18] Fiori L., "Propulsori MPD con Campo Magnetico Autoapplicato", *LAUREA Thesis in Ingegneria Aeronautica, Università degli Studi di Roma "La Sapienza",* a.a. 1996-1997 (In Italian).

[19] Ralli C., "Analisi Sperimentale del Campo Magnetico in Propulsori MPD", *LAUREA Thesis in Ingegneria Aeronautica, Università degli Studi di Roma "La Sapienza",* a.a. 1997-1998 (In Italian).

[20] Paccani G. and Ravignani R., "Sistema per la misura della spinta di propulsori MPD", *Aerotecnica, Missili e Spazio, Vol. 72, pp. 42-51, No. 1,* Jan-Jun 1994 (In Italian).

[21] Paccani G. and Di Zenzo S., "Computerized Jet Velocity Measurements in MPD Thrusters", *Aerotecnica, Missili e Spazio, vol 74, No. 3-4, pp. 93-102,* Jul-Dec 1995.

[22] Paccani G. and Petrucci L., "Self-Applied Magnetic Field Effects On Solid Propellant MPD Thruster Performance due to an Elongated Coil", *IEPC Paper 01-139, 27th IEPC, Pasadena, California (USA),* October 2001.